Metal Strip Endfire Antenna Based on TE_1 Leaky-Wave Mode

Libin Sun, *Student Member, IEEE*, Peiqin Liu, *Member, IEEE*, Yue Li, *Senior Member, IEEE*, Le Chang, Kunpeng Wei, *Senior Member, IEEE*, and Zhijun Zhang, *Fellow, IEEE*

***Abstract*— In this article, the guided-wave modes and leaky-wave characteristic of rectangular metal strips are investigated to realize endfire radiation. By strategically exciting the high-order TE_1 leaky-wave mode in the metal strip, a transverse in-phase *E*-field could be realized to generate an endfire radiation. An effective scheme is validated to manipulate the phase constant and leaky rate by altering the width of the TE_1 mode metal strip. Then, to further tailor the phase constant and leaky rate for achieving an enhanced directivity, periodic grooves are etched on both edges of the metal strip to slowdown the phase velocity to a surface-wave mode. To verify this concept, an all-metal planar prototype of corrugated rectangular metal strip (CRMS) was fabricated and measured. Both the full-wave simulation and experimental results show that the CRMS could offer a high endfire gain of 14.2 dBi within a footprint of $3.0 \times 0.5\lambda_0^2$. Moreover, a broad overlapping bandwidth of 27.7% is realized with $S_{11} < -10$ dB, gain variation less than 3 dB, and total efficiency better than 90%. The proposed design scheme paves the way for the traveling-wave antenna with simple structure, wide bandwidth, high gain, and good platform accommodation.**

***Index Terms*— Endfire antenna, high gain, leaky-wave antenna, metal strip, surface-wave antenna, traveling-wave antenna.**

I. Introduction

METAL surfaces are ubiquitous in almost all the platforms, such as airplanes, ships, vehicles, and the ground planes of the mobile terminals. By effectively exciting the metal surface on the platform as a major radiator, the antenna could be integrated with the platform to realize a dramatically enlarged radiation aperture and a reduced design complexity.

The theory of characteristic mode (TCM) provides an effective way to solve the natural eigenmodes of an arbitrary-shaped radiator or scatter independent of the external exciting source [1]–[4]. Consequently, TCM is widely employed in the platform-integrated antenna design by exciting the eigenmodes of the naval ship [5], unmanned aerial vehicle [6], shipboard [7], expeditionary fighting vehicle [8], military vehicle [9], and airplane [10]. Similarly, in the mobile terminal antennas [11], the characteristic modes of metal chassis and bezels are effectively excited to enhance the bandwidth [12]–[14]. However, for an electrical large metal surface that supports traveling-wave modes, TCM cannot offer an effective and accurate modal analysis with only resonant mode considered [4].

The surface-wave mode along an infinitely long single cylindrical conductor with finite conductivity has already been discussed by A. Sommerfeld in the early 1900s [15]. Then, Goubau [16] generalized Sommerfeld's wave by exploiting the modified metal conductor in 1950. In 2004, Pendry *et al.* [17] proposed a highly localized surface-wave mode in a metal block by drilling subwavelength holes in the microwave and terahertz spectrums to mimic the optical surface plasmon polaritons (SPPs), which is known as spoof SPPs (SSPPs). Recently, various SSPP transmission lines (TLs) with open waveguide structures are investigated to realize a low-loss transmission with a single conductor [18]–[22]. Furthermore, the SSPP TLs could be readily transformed to antennas by delocalizing the confined SSPP surface-wave mode into the leaky-wave mode [23], [24] with a conical [25], [26] or endfire [27]–[29] beam.

To effectively exploit the metal surfaces in various platforms, the guided-wave modes and leaky-wave characteristic of a single rectangular metal strip are investigated in this article. By strategically exciting the high-order TE_1 leaky-wave mode instead of the dominant quasi-TEM mode of the rectangular metal strip, a transverse in-phase fringe electric field (*E*-field) could be excited to achieve endfire radiation. Moreover, the phase constant and leaky rate of the TE_1 leaky-wave mode could be modulated by the width of the metal strip. Therefore, a moderate-gain endfire beam could be realized with a tailored phase constant and leaky rate. However, the fast-wave nature of the TE_1 mode, with an oblique array factor, will limit the enhancement of the antenna directivity. Therefore, to further shape the beam and enhance the antenna directivity, periodic shallow grooves are cut in both edges of the rectangular metal strip to slowdown the phase velocity to a surface-wave mode. Owing to the approximate satisfaction of the Hansen–Woodyard conditions [30], [31], an enhanced endfire gain of 14.8 dBi is realized within a small footprint of $3 \times 0.5\lambda_0^2$, which indicates an absolutely higher gain per unit area compared to the SSPP endfire antenna [27]–[29].

Manuscript received June 29, 2019; revised January 7, 2020; accepted April 3, 2020. Date of publication April 14, 2020; date of current version August 4, 2020. This work was supported by the National Natural Science Foundation of China under Contract 61971254 and Contract 61525104. *(Corresponding author: Zhijun Zhang.)*

Libin Sun, Yue Li, and Zhijun Zhang are with the Beijing National Research Center for Information Science and Technology (BNRist), Tsinghua University, Beijing 100084, China (e-mail: zjzh@tsinghua.edu.cn).

Peiqin Liu is with the Department of Electrical and Computer Engineering, National University of Singapore, Singapore 117583.

Le Chang and Kunpeng Wei are with Huawei Device Ltd., Beijing 100095, China.

Color versions of one or more of the figures in this article are available online at http://ieeexplore.ieee.org.

Digital Object Identifier 10.1109/TAP.2020.2986707

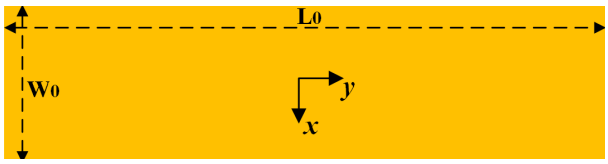

Fig. 1. Rectangular metal strip with a footprint of $3\lambda_0 \times 0.5\lambda_0$ at 3.5 GHz.

The rest of this article is organized as follows: In Section II, the operating modes, dispersion analysis, and radiation performance of an intact rectangular metal strip with both electric and magnetic excitations are demonstrated. In Section III, the operating mechanism and detailed parameter analysis of a corrugated rectangular metal strip (CRMS) are presented. In Section IV, the experimental verification is performed with the S-parameter, antenna gain, and radiation pattern considered. Finally, Section V draws a conclusion of this article.

II. Intact Rectangular Metal Strip

A. Modal Analysis by Electric and Magnetic Excitations

Fig. 1 shows the geometry of a PEC rectangular metal strip with a footprint of 3.0 $\lambda_0 \times$ 0.5 λ_0 (257 mm $\times$ 43 mm) at 3.5 GHz. To analyze the mode in the proposed rectangular metal strip, two different exciters, i.e., electric excitation and magnetic excitation, are applied to excite different guided-wave modes in the proposed rectangular metal strip.

The electric excitation is realized by a small metal sheet as shown in Fig. 2(a) and the feeding source is supplied between the metal sheet and the rectangular metal strip. Fig. 2(b) shows the corresponding vector E-field distribution in the xy plane. The electromagnetic wave is confined in the metal strip and propagates along the length with slight power leakage due to the open structure. The transverse vector E-field distribution in this manner, as shown in Fig. 2(c), exhibits a quasi-TEM mode. To have an intuitive insight of the dispersion characteristic of this mode, the simulated dispersion diagram is extracted from the full-wave simulation software HFSS as shown in Fig. 3. A good agreement is achieved between the proposed quasi-TEM mode and the light line ($\beta = k_0$). However, as shown in Fig. 2(c), the fringe E-fields at two edges of the metal strip are out of phase in this mode, leading to a radiation null at the endfire direction with a conical-like radiation beam.

In order to obtain a directional beam at the endfire direction, another excitation scheme is presented as shown in Fig. 2(d). By etching an electrical small slot in the metal strip and supplying feeding source at two sides of the slot, a high-order TE_1 leaky-wave mode with a center E-field null is realized as shown in Fig. 2(e) and (f). Different from the aforementioned quasi-TEM mode with out-of-phase E-field distribution, the fringe E-field is in phase in this manner, with the help of the transverse resonance, which could eliminate the radiation null at the propagating direction and generate an endfire beam. The theoretic phase constant β of the TE_1 leaky-wave mode could be approximately derived from the first high-order mode of the strip lines [32]

$$\beta_{TE1} = \sqrt{k_0^2 - (\pi / W_0)^2} \tag{1}$$

where k_0 is the wavenumber in the free space and W_0 is the width of the rectangular metal strip. The simulated dispersion diagram of the TE_1 leaky-wave mode is also in line with the theoretic result as illustrated in Fig. 3.

B. Radiation Performance of the TE_1 Mode Metal Strip

The fast-wave nature of the TE_1 mode metal strip, however, contributes to a rapidly growing leaky rate than the TEM mode. As shown in Fig. 2(e), the leaky rate of TE_1 leaky-wave mode is so severe that the power has almost been leaked away when it reaches the end of the metal strip. In order to obtain a large effective aperture and highly directional beam, it is crucial to control the leaky rate to an appropriate value. However, unlike the conventional leaky-wave antenna which could control the leaky rate by the size and position of the radiation elements [33], [34], the leaky rate of this open waveguide structure could only be controlled by manipulating the phase velocity. As we all know, the fast-wave ($\beta < k_0$) mode could effectively radiate the power, whereas the slow-wave ($\beta > k_0$) mode is hard to radiate the power even though the structure is open [23], [24]. As a result, by increasing the phase constant and slowing down the phase velocity, the leaky rate of the open waveguide can be decreased.

According to the dispersion equation (1), the phase constant β of the TE_1 mode could be easily manipulated by the transverse wavenumber, i.e., the width W_0 of the metal strip. Therefore, the leaky rate could also be controlled by altering W_0. Fig. 4 shows the simulated normalized phase constant and leaky rate versus the width W_0. As seen, with the increasing of W_0, the phase constant increases and the leaky rate decreases. Accordingly, with the mitigation of leaky rate, an enlarged radiation aperture and enhanced directivity could be achieved.

The beam pointing of the uniform leak-wave antenna could be approximately derived by

$$\sin\theta \cong \beta / k_0. \tag{2}$$

Thus, the beam pointing at both radiation edges of the rectangular metal strip is oblique due to the fast-wave ($\beta < k_0$) nature of the TE_1 leaky-wave mode. Fig. 5(a) shows the schematic of the beam pointing at both radiation edges with different widths W_0. The oblique angle is gradually mitigated with the expansion of W_0 due to the increase in the phase constant β. With the superposition of two symmetric oblique beams, an endfire beam with two large sidelobes is obtained as shown in Fig. 5(b). To suppress the back radiation, a square reflector is loaded at the backside as shown in the inset. With the increasing of W_0, the directivity is enhanced due to the mitigation of the leaky rate and the decline of the beam angle. The directivity reaches to 10.0 dBi when $W_0 = \lambda_0$. However, as shown in Fig. 4, the change rate of α and β slowdowns with the increasing of W_0, hence it is hard to further control the leaky rate and enhance the directivity by altering W_0.

It has been validated in theory by Hansen and Woodyard [30] and Balanis [31] that the theoretical maximum directivity could be realized when the phase constant β satisfy

$$(\beta - k_0)L \approx \pi \tag{3}$$

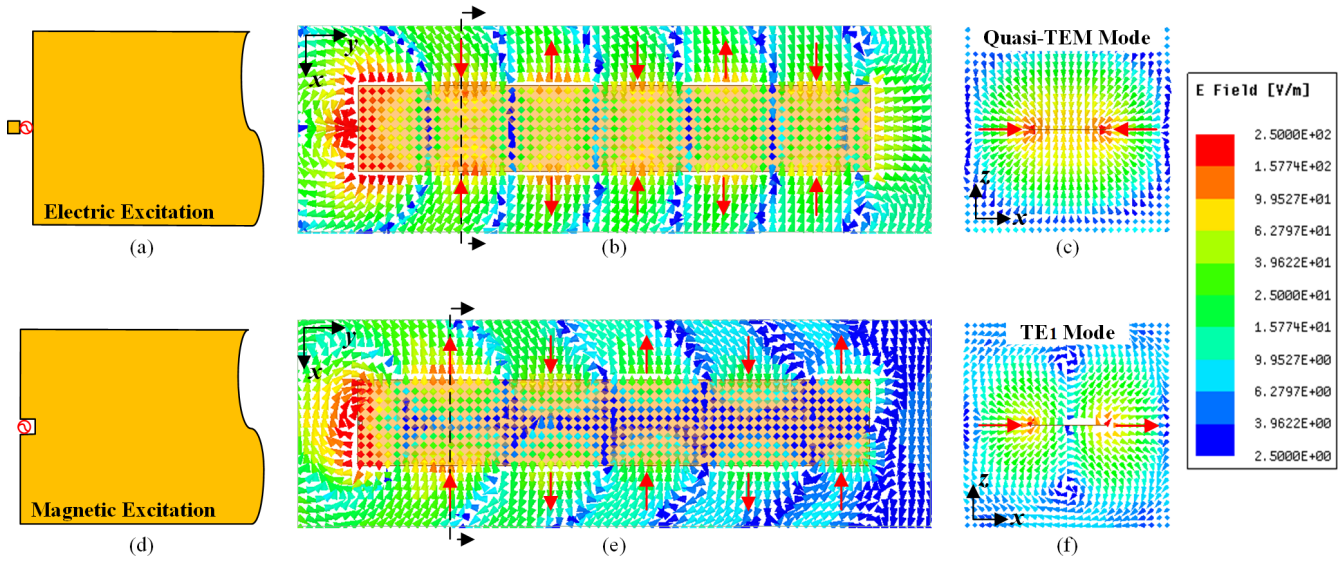

Fig. 2. Configurations of the exciter and corresponding E-field distributions for the proposed rectangular metal strip. (a) Configuration of the electric excitation. (b) Vector E-field distribution in the xy plane by the electric excitation. (c) Vector E-field distribution in the cross section (xz plane) by the electric excitation. (d) Configuration of the magnetic excitation. (e) Vector E-field distribution in the xy plane by the magnetic excitation. (f) Vector E-field distribution in the cross section (xz plane) by the magnetic excitation.

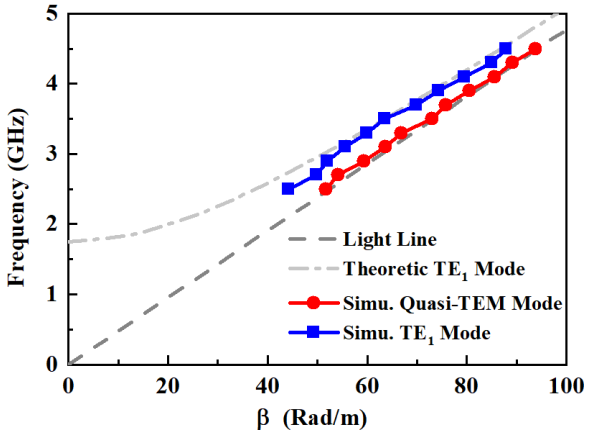

Fig. 3. Dispersion diagram of the calculated and simulated TEM and TE_1 leaky-wave modes of the proposed rectangular metal strip.

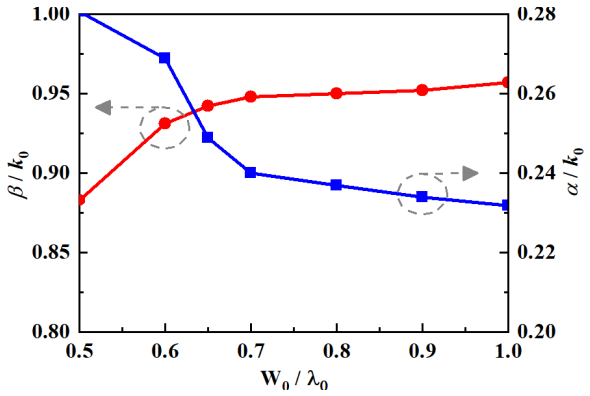

Fig. 4. Simulated normalized phase constant β/k_0 and leaky rate α/k_0 versus the width W_0.

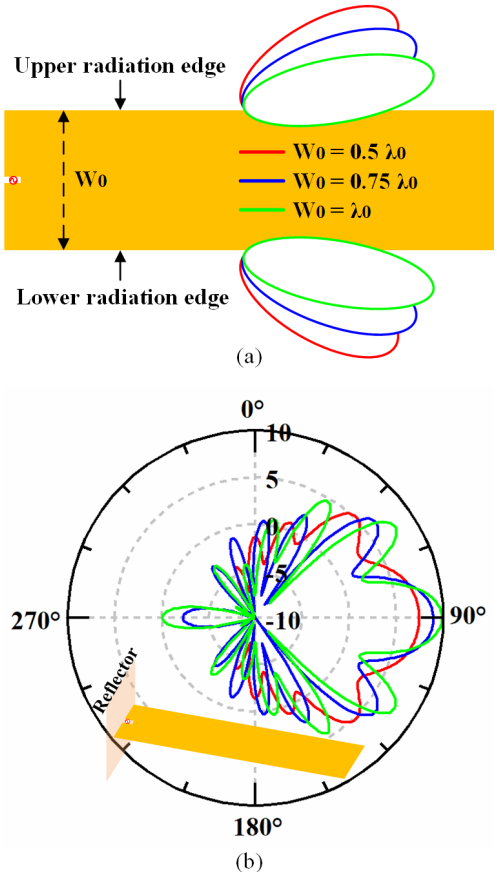

Fig. 5. (a) Schematic of the beam pointing at both radiation edges with different widths $W_0 = 0.5\lambda_0$, $0.75\lambda_0$, and λ_0. (b) Simulated radiation patterns with $W_0 = 0.5\lambda_0$, $0.75\lambda_0$, and λ_0, inset is the geometry of the magnetic-excited metal strip with a square reflector to suppress the backside radiation.

where L is the length of the array and k_0 is the wavenumber in the free space. According to (3), the phase velocity should be slightly slower than the speed of light for realizing a maximum directivity. However, the phase velocity of the TE_1 leaky-wave mode is always faster than the speed of light by simply increasing W_0. As a result, in order to enhance the endfire directivity further, some other approaches should be implemented to

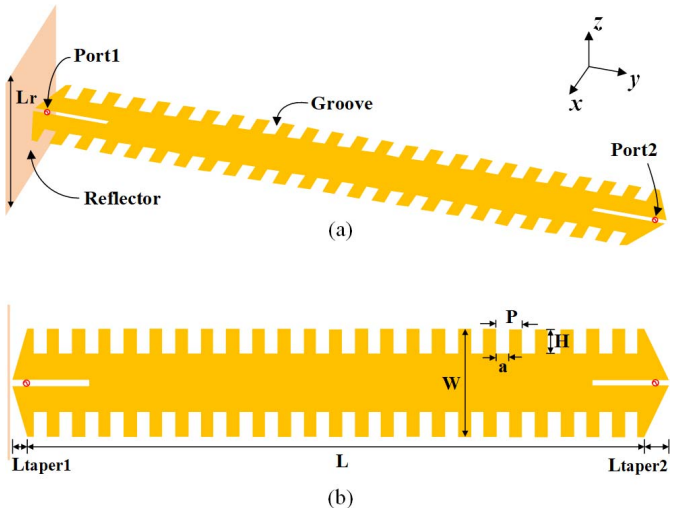

Fig. 6. Geometry of the CRMS. (a) Perspective view. (b) Top view.

TABLE I
DETAILED DIMENSIONS (UNIT: mm)

Parameter	L	L_{taper1}	L_{taper2}	W
Value	240	6	10	42
Parameter	L_r	H	P	a
Value	60	9.5	10	5

slowdown the phase velocity from a leaky-wave mode into a surface-wave mode.

III. CORRUGATED RECTANGULAR METAL STRIP

A. Antenna Structure

As shown in Fig. 6, periodic grooves are etched at both edges of the rectangular metal strip to further slowdown the phase velocity of the metal strip. Also, a square reflector is loaded behind to suppress the backside radiation. The CRMS is fed through Port1 by the magnetic excitation, while Port2 is matched by 50 Ω to absorb the residual power. Two taper transitions are implemented at both sides of the CRMS to realize a smooth transition and reduce the power reflection. The whole dimension of the CRMS still remains $3.0\lambda_0 \times 0.5\lambda_0$ at 3.5 GHz for comparison. The parameters are optimized in full-wave simulation software HFSS and the detailed dimensions are listed in Table I.

B. Modal and Dispersion Analysis

To offer an intuitive insight of the proposed CRMS, the E-field distribution is illustrated in Fig. 7. As shown in Fig. 7(a), the E-field distribution in the transverse almost keeps unchanged with a TE_1-like mode due to the little impact of the subwavelength grooves. On the contrary, the phase constant and leaky rate in the propagating direction, as shown in Fig. 7(b), are dramatically changed with the extension of the traveling-wave current path due to the load of periodic grooves. To quantitatively analyze the impact of the grooves, the simulated normalized phase and leaky constants are demonstrated in Fig. 8. The depth H of the grooves

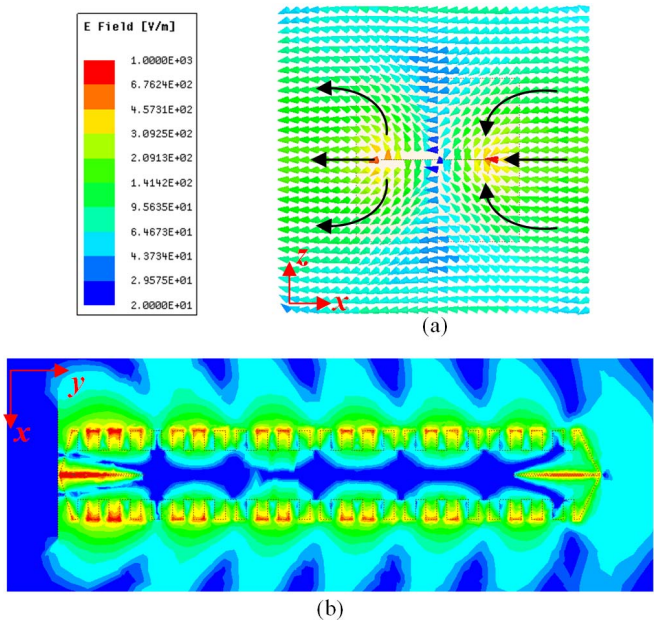

Fig. 7. Simulated E-field distribution of the CRMS at 3.5 GHz. (a) Vector E-field distribution in the cross section (xz plane). (b) E-field distribution in the xy plane.

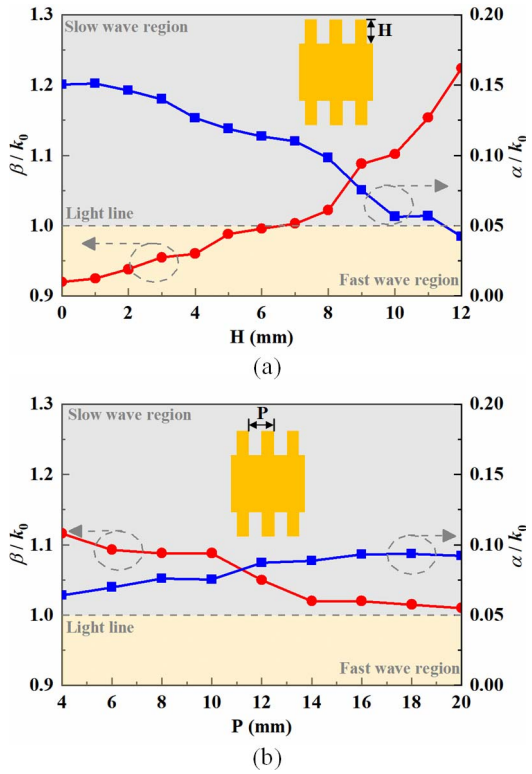

Fig. 8. (a) Simulated normalized phase constant and leaky rate with the impact of the depth H of the grooves when $P = 2a = 10$ mm. (b) Simulated normalized phase constant and leaky rate with the impact of the periodic P of the grooves when $H = 9.5$ mm and $a = P/2$.

performs a tremendous impact on the phase constant and leaky rate as shown in Fig. 8(a). With the increasing of H, the phase constant increases from the fast-wave region into the slow-wave region; meanwhile, the leaky rate is gradually reduced with a confined field in the surface. The periodic P of the grooves, as shown in Fig. 8(b), also affects the

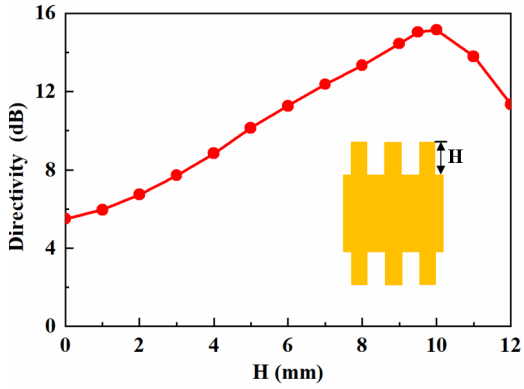

Fig. 9. Simulated directivity of the CRMS at 3.5 GHz versus the depth H of the periodic grooves.

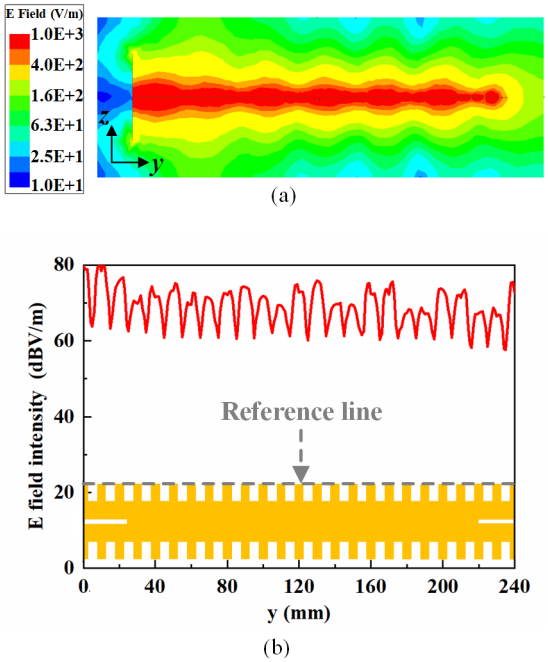

Fig. 10. Simulated E-field distribution of the proposed CRMS at 3.5 GHz. (a) Complex E-field amplitude distribution in the yz plane. (b) E-field intensity along the reference line shown in the inset.

phase constant and leaky rate because the number of etching grooves is changed with the variation of periodic P. However, the impact of the periodic P is not as dramatic as the depth H.

C. Radiation Performance

With a tremendous manipulation of the phase constant and leaky rate, the depth H is the key factor to improve the directivity of the metal strip. As illustrated in Fig. 9, the directivity gradually rises with the increasing of H and reaches to a maximum value of 15.1 dBi when $H = 9.5$ mm. In this point, the normalized phase constant $\beta/k_0 = 1.095$ rad/m and the normalized leaky rate $\alpha/k_0 = 0.66$ rad/m, which indicate a slow-wave mode with a suitable power leakage to approximately satisfy the Hansen–Woodyard conditions.

Different from the conventional traveling-wave antennas with an exponentially decayed E-field distribution along the array [23], [24], the proposed CRMS has a uniform E-field distribution along the length due to the surface-wave transmission as shown in Fig. 10(a). The absolute E-field intensity along the reference line (shown in the inset) is also depicted in Fig. 10(b) to quantitatively exhibit the uniformity of the E-fields.

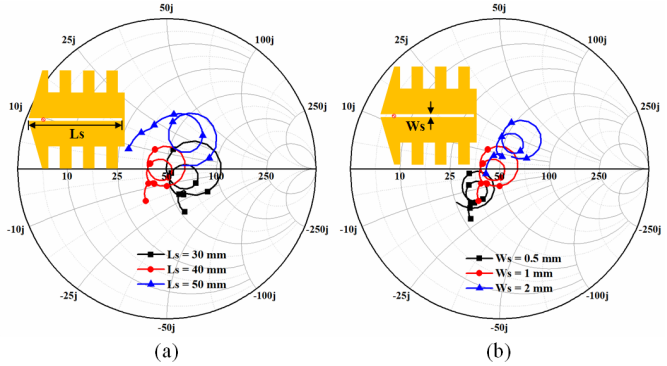

Fig. 11. Simulated normalized Smith chart (S_{11}) with different values of (a) Ls and (b) Ws.

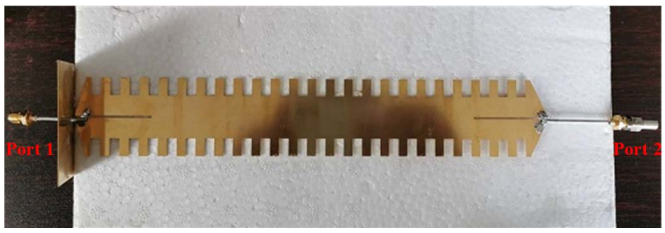

Fig. 12. Photographs of the proposed CRMS. The antenna is fed through Port1 and matched at Port2.

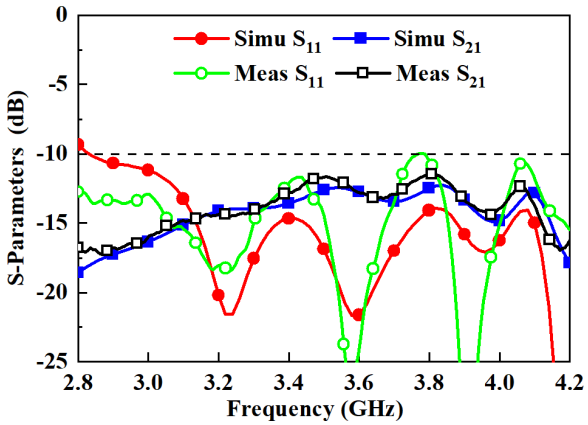

Fig. 13. Simulated and measured reflection coefficients and transmission coefficients of the proposed CRMS.

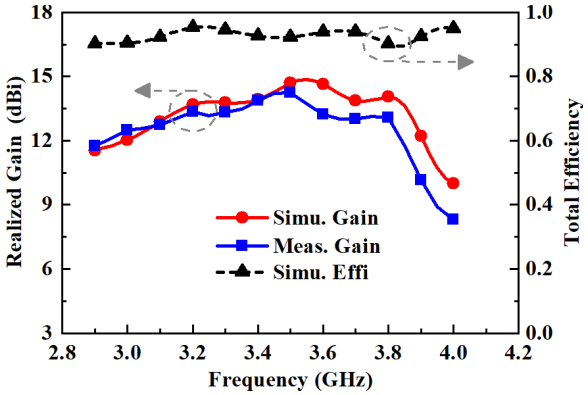

Fig. 14. Simulated and measured endfire gains and simulated total efficiency for the proposed CRMS.

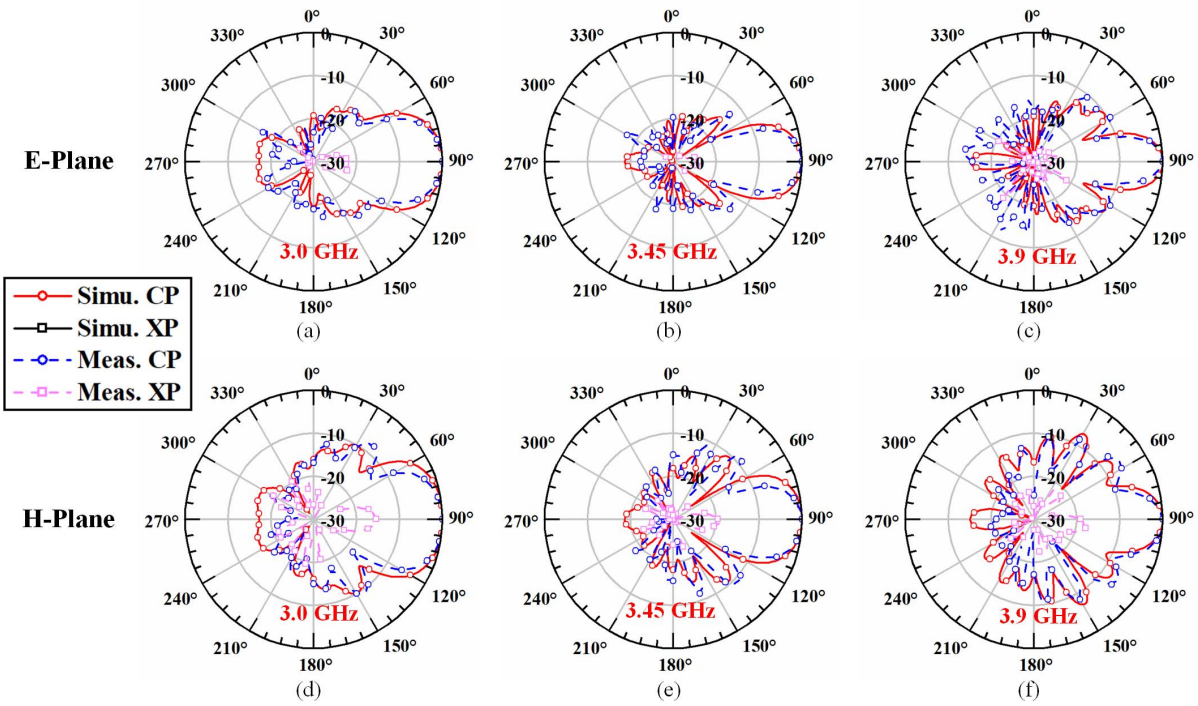

Fig. 15. Simulated and measured normalized radiation patterns in the E-plane (*xoy* plane) and the H-plane (*yoz* plane). (a) E-plane at 3.0 GHz. (b) E-plane at 3.45 GHz. (c) E-plane at 3.9 GHz. (d) H-plane at 3.0 GHz. (e) H-plane at 3.45 GHz. (f) H-plane at 3.9 GHz.

D. Impedance Matching

To achieve a good impedance matching, the length Ls and width Ws of the feeding slot are tuned for an optimized bandwidth response. Fig. 11(a) shows the Smith chart of the reflection coefficient with different values of Ls. The slot line could be equivalent to a terminal short-circuit TL, thus the input impedance could be altered by tuning the length Ls. Fig. 11(b) shows the Smith chart of the reflection coefficient with different values of Ws. With the increasing of Ws, the capacitance effect of the slot line is decreased with a shift from the capacitive region to the inductive region in the Smith chart. The final optimized parameters of the feeding slot are $L\text{s} = 40$ mm and $W\text{s} = 1$ mm with a -10 dB impedance bandwidth of 2.83–4.60 GHz.

IV. Experimental Verification

To validate the performance of the proposed CRMS, an all-metal prototype was fabricated as shown in Fig. 12. The antenna is manufactured by the standard laser cutting process on a 0.5 mm-thick brass plate ($\sigma = 1.5 \times 10^7$ S/m). The antenna is fed through Port1 by a 50 Ω semirigid cable with outer conductor soldered at one side of the feeding slot and inner conductor soldered at another side. In the end, a 50 Ω matched load is connected at Port2 to absorb the residual power.

A. S-Parameters

The simulated and measured reflection coefficients and transmission coefficients are presented in Fig. 13. The simulated and measured results are in a good agreement, which indicate a wide -10 dB impedance bandwidth from 2.8 to 4.2 GHz (40.0%) and an effective power leakage with $S_{21} < -11.5$ dB across the desired band.

B. Radiation Performance

The simulated and measured gains at the endfire direction are reported in Fig. 14. The simulated maximum gain is 14.8 dBi at 3.55 GHz, whereas the measured result is 14.2 dBi at 3.50 GHz. In addition, a good gain stability with the simulated 3 dB gain bandwidth from 2.97 to 3.91 GHz (26.8%) and the measured 3 dB gain bandwidth from 2.90 to 3.87 GHz (27.7%) is realized. Thanks to the all-metal strategy with a negligible dielectric and metal loss, a high antenna efficiency of better than 90.0% is realized as exhibited in Fig. 14.

To demonstrate the radiation characteristic of the proposed CRMS, the simulated and measured normalized radiation patterns in the E- and H-planes at 3.0, 3.45, and 3.9 GHz are presented in Fig. 15. A stable radiation pattern with a highly directional endfire beam is realized. The main beams are narrowed with the increase in frequency due to the expansion of the electrical length. The measured half-power beam widths (HPBWs) at 3.0, 3.45, and 3.9 GHz are 35°, 25°, and 18° in the E-plane and 44°, 31°, and 26° in the H-plane, respectively. With the planar structure, the cross-polarization (XP) is low with XP discriminations better than 30 dB in simulation and 15 dB in measurement. Moreover, due to the forward traveling-wave mode and the load of the reflector, the front-to-back ratio levels at 3.0, 3.45, and 3.9 GHz are 31, 26, and 16 dB in the E-plane and 24, 26, and 21 dB in the H-plane, respectively.

TABLE II
COMPARISONS WITH THE SSPP ENDFIRE ANTENNAS

Ref.	L×W (λ_0^2)	Overlapping bandwidth[a]	Maximum gain (dBi)	G/A[b] ($1/\lambda_0^2$)
[27]	2.85×0.32	>12.5%	9.2	9.12
[28]	3.65×0.53	~14.3%	11.3	6.97
[29]	1.36×0.86	~50%	8.6	6.19
Our Work	3.0×0.49	27.7%	14.2	17.90

[a] Overlapping bandwidth with S_{11} < -10 dB and gain variation < 3dB.
[b] Gain per unit area (G/A) is defined as the absolute realized gain value per wavelength square area.

V. CONCLUSION

This article offers a new insight of the guided-wave modes and leaky-wave characteristic of a single rectangular metal strip. By strategically exciting the high-order TE_1 leaky-wave mode in the metal strip, a high-gain endfire radiation could be realized with the in-phase E-field in the transverse. From the intact metal strip to the corrugated metal strip, the phase constant and leaky rate could be well tailored to achieve a uniform aperture and an enhanced gain with the approximate satisfaction of the Hansen–Woodyard conditions.

Both the simulation and measurement results demonstrate that the proposed corrugated metal strip could offer a high endfire gain of 14.8 dBi in simulation and 14.2 dBi in measurement. In addition, a wide bandwidth response of 27.7% is obtained with reflection coefficient less than -10 dB and gain variation less than 3 dB. Compared to the SSPP endfire antennas with tapering or fish-bone structures [27]–[29], our design scheme exhibits a higher gain and aperture efficiency as clearly shown in Table II. Compared to the up-to-date endfire antennas [36]–[40], the proposed design scheme not only has a higher gain within a smaller aperture but also possesses a simple structure and better platform accommodation with a single metal strip. We envision that our design scheme could offer an effective solution for the planar wideband and high-gain endfire antenna with a simple antenna structure and promising platform accommodation.

REFERENCES

[1] R. Garbacz and R. Turpin, "A generalized expansion for radiated and scattered fields," *IEEE Trans. Antennas Propag.*, vol. AP-19, no. 3, pp. 348–358, May 1971.

[2] R. Harrington and J. Mautz, "Computation of characteristic modes for conducting bodies," *IEEE Trans. Antennas Propag.*, vol. AP-19, no. 5, pp. 629–639, Sep. 1971.

[3] R. Harrington and J. Mautz, "Theory of characteristic modes for conducting bodies," *IEEE Trans. Antennas Propag.*, vol. AP-19, no. 5, pp. 622–628, Sep. 1971.

[4] Y. Chen and C. F. Wang, *Characteristic Modes: Theory and Applications in Antenna Engineering*. Hoboken, NJ, USA: Wiley, 2015.

[5] G. Marrocco and L. Mattioni, "Naval structural antenna systems for broadband HF communications," *IEEE Trans. Antennas Propag.*, vol. 54, no. 4, pp. 1065–1073, Apr. 2006.

[6] Y. Chen and C.-F. Wang, "Electrically small UAV antenna design using characteristic modes," *IEEE Trans. Antennas Propag.*, vol. 62, no. 2, pp. 535–545, Feb. 2014.

[7] Y. Chen and C.-F. Wang, "HF band shipboard antenna design using characteristic modes," *IEEE Trans. Antennas Propag.*, vol. 63, no. 3, pp. 1004–1013, Mar. 2015.

[8] T.-Y. Shih and N. Behdad, "Bandwidth enhancement of platform-mounted HF antennas using the characteristic mode theory," *IEEE Trans. Antennas Propag.*, vol. 64, no. 7, pp. 2648–2659, Jul. 2016.

[9] R. Ma, T.-Y. Shih, R. Lian, and N. Behdad, "Design of bandwidth-enhanced platform-mounted electrically small VHF antennas using the characteristic-mode theory," *IEEE Antennas Wireless Propag. Lett.*, vol. 17, no. 12, pp. 2384–2388, Dec. 2018.

[10] R. Ma and N. Behdad, "Design of platform-based HF direction-finding antennas using the characteristic mode theory," *IEEE Trans. Antennas Propag.*, vol. 67, no. 3, pp. 1417–1427, Mar. 2019.

[11] Z. Zhang, *Antenna Design for Mobile Devices*, 2nd ed. Hoboken, NJ, USA: Wiley, 2017.

[12] Z. Miers, H. Li, and B. K. Lau, "Design of bandwidth-enhanced and multiband MIMO antennas using characteristic modes," *IEEE Antennas Wireless Propag. Lett.*, vol. 12, pp. 1696–1699, Nov. 2013.

[13] C. Deng, Z. Feng, and S. V. Hum, "MIMO mobile handset antenna merging characteristic modes for increased bandwidth," *IEEE Trans. Antennas Propag.*, vol. 64, no. 7, pp. 2660–2667, Jul. 2016.

[14] C. Deng, Z. Xu, A. Ren, and S. V. Hum, "TCM-based bezel antenna design with small ground clearance for mobile terminals," *IEEE Trans. Antennas Propag.*, vol. 67, no. 2, pp. 745–754, Feb. 2019.

[15] J. A. Stratton, *Electromagnetic Theory*. New York, NY, USA: McGraw-Hill, 1941.

[16] G. Goubau, "Surface wave and their application to transmission lines," *J. Appl. Phys.*, vol. 21, no. 11, pp. 1119–1128, 1950.

[17] J. B. Pendry, "Mimicking surface plasmons with structured surfaces," *Science*, vol. 305, no. 5685, pp. 847–848, Aug. 2004.

[18] S. A. Maier, S. R. Andrews, L. Martín-Moreno, and F. J. García-Vidal, "Terahertz surface plasmon-polariton propagation and focusing on periodically corrugated metal wires," *Phys. Rev. Lett.*, vol. 97, no. 17, Oct. 2006, Art. no. 176805.

[19] C. R. Williams, S. R. Andrews, S. A. Maier, A. I. Fernández-Domínguez, L. Martín-Moreno, and F. J. García-Vidal, "Highly confined guiding of terahertz surface plasmon polaritons on structured metal surfaces," *Nature Photon.*, vol. 2, no. 3, pp. 175–179, Mar. 2008.

[20] X. Shen, T. J. Cui, D. Martin-Cano, and F. J. Garcia-Vidal, "Conformal surface plasmons propagating on ultrathin and flexible films," *Proc. Nat. Acad. Sci. USA*, vol. 110, no. 1, pp. 40–45, Jan. 2013.

[21] A. Kianinejad, Z. N. Chen, and C.-W. Qiu, "Design and modeling of spoof surface plasmon modes-based microwave slow-wave transmission line," *IEEE Trans. Microw. Theory Techn.*, vol. 63, no. 6, pp. 1817–1825, Jun. 2015.

[22] A. Kianinejad, Z. N. Chen, and C.-W. Qiu, "Low-loss spoof surface plasmon slow-wave transmission lines with compact transition and high isolation," *IEEE Trans. Microw. Theory Techn.*, vol. 64, no. 10, pp. 3078–3086, Oct. 2016.

[23] D. R. Jackson and A. A. Oliner, "Leaky-wave antennas," in *Modern Antenna Handbook*, C. A. Balanis, Ed. Hoboken, NJ, USA: Wiley, vol. 2008, ch. 7.

[24] D. R. Jackson, C. Caloz, and T. Itoh, "Leaky-wave antennas," *Proc. IEEE*, vol. 100, no. 7, pp. 2194–2206, Jul. 2012.

[25] G. S. Kong, H. F. Ma, B. G. Cai, and T. J. Cui, "Continuous leaky-wave scanning using periodically modulated spoof plasmonic waveguide," *Sci. Rep.*, vol. 6, no. 1, Sep. 2016, Art. no. 29600.

[26] F. A. Kianinejad, Z. N. Chen, and C.-W. Qiu, "A single-layered spoof plasmon-mode leaky wave antenna with consistent gain," *IEEE Trans. Antennas Propag.*, vol. 65, no. 2, pp. 681–687, Nov. 2017.

[27] A. Kandwal, Q. Zhang, X.-L. Tang, L. W. Liu, and G. Zhang, "Low-profile spoof surface plasmon polaritons traveling-wave antenna for near-endfire radiation," *IEEE Antennas Wireless Propag. Lett.*, vol. 17, no. 2, pp. 184–187, Feb. 2018.

[28] Y. Han *et al.*, "Endfire antennas based on spoof surface plasmon," in *Proc. Int. Appl. Comput. Electromagn. Soc. Symp. (ACES)*, Suzhou, China, Aug. 2017, pp. 1–2.

[29] X. Du, H. Li, and Y. Yin, "Wideband fish-bone antenna utilizing odd-mode spoof surface plasmon polaritons for end-fire radiation," *IEEE Trans. Antennas Propag.*, vol. 67, no. 7, pp. 4848–4853, Jul. 2019.

[30] W. W. Hansen and J. R. Woodyard, "A new principle in directional antenna design," *Proc. IRE*, vol. 26, no. 3, pp. 333–345, Mar. 1938.

[31] C. A. Balanis, *Antenna Theory Analysis and Design*, 3rd ed. Hoboken, NJ, USA: Wiley, 2005.

[32] D. M. Pozar, *Microwave Engineering*, 2nd ed. New York, NY, USA: Wiley, 1998.

[33] L. Sun, Y. Hou, Y. Li, Z. Zhang, and Z. Feng, "An open cavity leaky-wave antenna with vertical-polarization endfire radiation," *IEEE Trans. Antennas Propag.*, vol. 67, no. 5, pp. 3455–3460, May 2019.

[34] J. Liu, D. R. Jackson, Y. Li, C. Zhang, and Y. Long, "Investigations of SIW leaky-wave antenna for endfire-radiation with narrow beam and sidelobe suppression," *IEEE Trans. Antennas Propag.*, vol. 62, no. 9, pp. 4489–4497, Sep. 2014.
[35] X.-F. Zhang, J. Fan, and J.-X. Chen, "High gain and high-efficiency millimeter-wave antenna based on spoof surface plasmon polaritons," *IEEE Trans. Antennas Propag.*, vol. 67, no. 1, pp. 687–691, Jan. 2019.
[36] P. Liu, H. Feng, Y. Li, and Z. Zhang, "Low-profile EndFire leaky-wave antenna with air media," *IEEE Trans. Antennas Propag.*, vol. 66, no. 3, pp. 1086–1092, Mar. 2018.
[37] P. Liu, Y. Li, Z. Zhang, and P. Jia, "All-metal centipede-like end-fire antenna," *IEEE Antennas Wireless Propag. Lett.*, vol. 17, no. 10, pp. 1905–1908, Oct. 2018.
[38] Y. Hou, Y. Li, Z. Zhang, and Z. Feng, "Narrow-width periodic leaky-wave antenna array for endfire radiation based on Hansen–Woodyard condition," *IEEE Trans. Antennas Propag.*, vol. 66, no. 11, pp. 6393–6396, Nov. 2018.
[39] Y. Hou, Y. Li, Z. Zhang, and M. F. Iskander, "All-metal endfire antenna with high gain and stable radiation pattern for the platform-embedded application," *IEEE Trans. Antennas Propag.*, vol. 67, no. 2, pp. 730–737, Feb. 2019.
[40] Y. Hou, Y. Li, Z. Zhang, and Z. Feng, "A broadband and high-gain endfire antenna array fed by air-substrate parallel strip line," *IEEE Trans. Antennas Propag.*, vol. 67, no. 8, pp. 5717–5722, Aug. 2019.

Libin Sun (Student Member, IEEE) received the B.S. degree from Xidian University, Xi'an, China, in 2016. He is currently pursuing the Ph.D. degree with the Department of Electrical and Engineering, Tsinghua University, Beijing, China.

His current research interests include antenna design and theory, particularly in 5G terminal antennas, MIMO and diversity antennas, circularly polarized antennas, and leaky-wave and surface-wave antennas.

Mr. Sun was a recipient of the Top 50 Outstanding Reviewer Award of the IEEE TRANSACTIONS ON ANTENNAS AND PROPAGATION in 2019. He serves as a Reviewer for the IEEE TRANSACTIONS ON ANTENNAS AND PROPAGATION, the IEEE ANTENNAS AND WIRELESS PROPAGATION LETTERS, IEEE ACCESS, *IET Electronics Letters*, *Microwave and Optical Letters*, and the *International Journal of RF and Microwave Computer-Aided Engineering*.

Peiqin Liu (Member, IEEE) received the B.S. degree from the University of Electronic Science and Technology of China, Chengdu, China, in 2014 and the Ph.D. degree in electronic engineering from Tsinghua University, Beijing, China, in 2019.

Since September 2019, he has been with the National University of Singapore, Singapore, where he is currently a Research Fellow. His current research interests include metamaterials and antenna theory, particularly in novel metasurface with artificial intelligence methods.

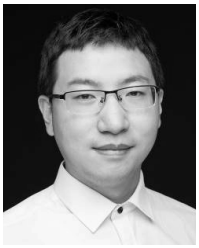

Yue Li (Senior Member, IEEE) received the B.S. degree in telecommunication engineering from Zhejiang University, Zhejiang, China, in 2007 and the Ph.D. degree in electronic engineering from Tsinghua University, Beijing, China, in 2012.

In June 2012, he was a Post-Doctoral Fellow with the Department of Electronic Engineering, Tsinghua University, where he is currently an Associate Professor. In December 2013, he was a Research Scholar with the Department of Electrical and Systems Engineering, University of Pennsylvania, Philadelphia, PA, USA. He was also a Visiting Scholar with the Institute for Infocomm Research (I2R), A∗STAR, Singapore, in 2010 and the Hawaii Center of Advanced Communications (HCAC), University of Hawai'i at Mānoa, Honolulu, HI, USA, in 2012. Since January 2016, he has been with Tsinghua University. He has authored or coauthored over 90 journal articles and 45 international conference papers, and holds 15 granted Chinese patents. His current research interests include metamaterials, plasmonics, electromagnetics, nanocircuits, mobile and handset antennas, MIMO and diversity antennas, and millimeter-wave antennas and arrays.

Dr. Li serves as an Editorial Board Member of Scientific Report. He was a recipient of the Issac Koga Gold Medal from the URSI General Assembly in 2017; the Second Prize of Science and Technology Award of the China Institute of Communications in 2017; the young scientist awards from the conferences of the Applied Computational Electromagnetics Society (ACES) 2018, the URSI Atlantic Radio Science Conference (AT-RASC) 2018, the URSI Asia-Pacific Radio Science Conference (AP-RASC) 2016, the International Symposium on Electromagnetic Theory (EMTS) 2016, and URSI GASS 2014; the best paper awards from the conferences of the Cross Strait Quad-Regional Radio Science and Wireless Technology Conference (CSQRWC) 2018, the National Conference on Microwave and Millimeter Wave Technology (NCMMW) 2018 and 2017, the Asia-Pacific Conference on Antennas and Propagation (APCAP) 2017, the National Conference on Antenna (NCANT) 2017, the International Symposium on Antennas, Propagation and EM Theory (ISAPE) 2016, and the IEEE International Conference on Microwave and Millimeter Wave Technology (ICMMT) 2016; the Outstanding Doctoral Dissertation of Beijing Municipality in 2013; and the Principal Scholarship of Tsinghua University in 2011. He is serving as an Associate Editor for the IEEE TRANSACTIONS ON ANTENNAS AND PROPAGATION, the IEEE ANTENNAS AND WIRELESS PROPAGATION LETTERS, and *Computer Applications in Engineering Education*.

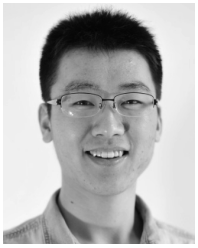

Le Chang received the B.S. degree in electronics and information engineering from Xidian University, Xi'an, China, in 2012 and the Ph.D. degree in electrical engineering from Tsinghua University, Beijing, China, in 2017.

He is currently working as a Senior Engineer with Huawei Device Ltd., Beijing.

Kunpeng Wei (Senior Member, IEEE) received the B.S. degree in electronic and information engineering from the Huazhong University of Science and Technology, Wuhan, China, in 2008 and the Ph.D. degree in electrical engineering from Tsinghua University, Beijing, China, in 2013.

From 2013 to 2016, he was employed with the Radar Research Institute of Chinese Air Force Research Laboratory, Beijing, where he conducted research in the areas of phased-array antenna design and radar system design. Since 2016, he has been working for the Consumer Business Group, Huawei Device Ltd., Beijing, as a Smart-Phone Antenna Expert. He has authored more than 20 technical articles on omnidirectional antenna design and MIMO antenna design and holds more than eight Patent Cooperation Treaty (PCT)-patents as the first inventor. His current research interests include smart-phone antenna design, small size 5G antenna systems in terminal device, and millimeter-wave antenna array.

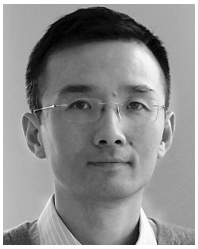

Zhijun Zhang (Fellow, IEEE) received the B.S. and M.S. degrees from the University of Electronic Science and Technology of China, Chengdu, China, in 1992 and 1995, respectively, and the Ph.D. degree from Tsinghua University, Beijing, China, in 1999.

In 1999, he was a Post-Doctoral Fellow with the Department of Electrical Engineering, The University of Utah, Salt Lake City, UT, USA, where he was appointed as a Research Assistant Professor in 2001. In May 2002, he was an Assistant Researcher with the University of Hawai'i at Mānoa, Honolulu, HI, USA. In November 2002, he joined Amphenol T&M Antennas, Vernon Hills, IL, USA, as a Senior Staff Antenna Development Engineer, where he was then promoted to the position of an Antenna Engineer Manager. In 2004, he joined Nokia Inc., San Diego, CA as a Senior Antenna Design Engineer. In 2006, he joined Apple Inc., Cupertino, CA, USA, as a Senior Antenna Design Engineer, where he was then promoted to the position of a Principal Antenna Engineer. Since August 2007, he has been with Tsinghua University, where he is currently a Professor with the Department of Electronic Engineering. He is the author of *Antenna Design for Mobile Devices* (Wiley, First Edition 2011, Second Edition 2017).

Dr. Zhang served as an Associate Editor for the IEEE TRANSACTIONS ON ANTENNAS AND PROPAGATION from 2010 to 2014 and the IEEE ANTENNAS AND WIRELESS PROPAGATION LETTERS from 2009 to 2015.